

A probabilistic assessment of sea level variations within the Last Interglacial stage

Robert E. Kopp^{1*}, Frederik J. Simons², Jerry X. Mitrovica³,
Adam C. Maloof² and Michael Oppenheimer^{2,4}

¹ *Department of Earth & Planetary Sciences and Rutgers Energy Institute, Rutgers University, Piscataway, NJ 08854, USA*

² *Department of Geosciences, Princeton University, Princeton, NJ 08544, USA*

³ *Department of Earth and Planetary Sciences, Harvard University, Cambridge, MA 02138, USA*

⁴ *Woodrow Wilson School of Public and International Affairs, Princeton University, Princeton, NJ 08544, USA*

This is the authors' preprint version of the manuscript: 23 January 2013. Originally submitted 18 September 2012.

SUMMARY

The Last Interglacial (LIG) stage (ca. 130–115 ka) provides a relatively recent example of a world with both poles characterized by greater-than-Holocene temperatures similar to those expected later in this century under a range of greenhouse gas emission scenarios. Previous analyses inferred that LIG mean global sea level (GSL) peaked 6–9 m higher than today (Kopp et al. 2009; Dutton & Lambeck 2012). Here, we extend our earlier work to perform a probabilistic assessment of sea level variability *within* the LIG highstand. Using the terminology for probability employed in the Intergovernmental Panel on Climate Change (IPCC) assessment reports, we find it extremely likely (95% probability) that the paleo-sea level record allows resolution of at least two intra-LIG sea level peaks and likely (67% probability) that the magnitude of low-to-high swings exceeded 4 m. Moreover, it is likely that there was a period during the LIG in which GSL rose at a 1000-year average rate exceeding 3 m/ky, but unlikely (33% probability) that the rate exceeded 7 m/ky and extremely unlikely (5% probability) that it exceeded 11 m/ky. These rate estimates can provide insight into rates of Greenland and/or Antarctic melt under climate conditions partially analogous to those expected in the twenty-first century.

Key words: sea level, Last Interglacial, Eemian, Antarctic ice sheet, Greenland ice sheet

1 INTRODUCTION

The Last Interglacial stage (LIG; ca. 130–115 ka) has attracted considerable interest from climate researchers, as it is the most recent Pleistocene interval during which temperatures at both poles and global mean temperature exceeded their Holocene levels. Ice core data suggest that LIG Greenland temperatures peaked about 5°C warmer than today (Andersen et al. 2004; CAPE-Last Interglacial

Project Members 2006; Otto-Bliesner et al. 2006) and that Antarctic temperatures were about 3–5°C warmer than pre-Industrial temperatures (Overpeck et al. 2006). Analyses of paleo-temperature data suggest that global mean temperature was ~1.5°C warmer than today (Turney & Jones 2010) and that global mean sea surface temperature (SST) was $0.7 \pm 0.6^\circ\text{C}$ warmer than pre-Industrial conditions (and hence about $0.2 \pm 0.6^\circ\text{C}$ warmer than today; NOAA National Climatic Data Center 2011) (McKay et al. 2011). (It is unclear whether the global mean temperature and global mean SST esti-

* Corresponding author. Email: robert.kopp@rutgers.edu

mates are consistent. McKay et al. (2011) have suggested that the global mean temperature estimate is biased toward terrestrial Northern Hemisphere summer temperatures.) Although the interpretation of the LIG as an analog for a future warmer climate is complicated by differences in insolation resulting from a more eccentric orbit (van de Berg et al. 2011), the Last Interglacial stage provides an accessible natural experiment for assessing the impact of warmer polar temperatures on ice sheet volumes and sea level.

Geological proxies for local paleo-sea level come from a variety of sources, including corals and coral reef terraces, sedimentary and biological facies, constructional and erosional terraces, and hydrological modeling of oxygen isotope records in semi-enclosed basins. The global marine benthic oxygen isotope record (Lisiecki & Raymo 2005) complements these local sea level records with an entangled joint proxy for benthic temperature and global ice volume. While, for small changes, mean global sea level (GSL) varies almost linearly with the total loss of land ice, the relationship between land ice mass and local sea level involves complex physical linkages. Notably, the redistribution of mass from land ice to the global ocean alters Earth’s gravitational field, topography and rotational state. In the short term, these effects lead to a significant sea level fall near the margins of a melting ice sheet and enhance sea level rise far from the ice sheet by up to $\sim 30\%$ relative to the global mean (Mitrovica et al. 2011); over thousands of years, these effects relax, as solid Earth deformations isostatically compensate for the surface mass (ice plus water) redistribution (Mitrovica & Milne 2003). Superimposed on these “static equilibrium sea level” effects are sea level changes driven by ocean dynamics and temperature and salinity distribution, although these “dynamic sea level” changes are dwarfed by static equilibrium effects resulting from glacial-interglacial swings in ice sheet volume for GSL changes in excess of ~ 20 cm (Kopp et al. 2010).

Kopp et al. (2009) (henceforth K09) employed a Bayesian statistical framework that coupled a database of LIG local paleo-sea level records from 47 localities with the global oxygen isotope record of Lisiecki & Raymo (2005) and a geophysical model of the static equilibrium response of local sea level to ice volume redistribution. We found that LIG GSL peaked considerably higher than today. Using terminology adopted in Intergovernmental Panel on Climate Change (IPCC) assessment reports, we concluded that a rise in LIG GSL ≥ 6.6 m was extremely likely (95% probability), a rise ≥ 8.0 m was likely (67% probability), and that a rise ≥ 9.4 m was unlikely (33% probability). Our result was subsequently confirmed by Dutton & Lambeck (2012) in an independent analysis that employed a different methodology and database but also estimated that

LIG GSL peaked between 5.5 and 9 m higher than today.

Local sea level indicators from several sites, including the Bahamas (Chen et al. 1991; Hearty et al. 2007; Thompson et al. 2011), the Yucatán (Blanchon et al. 2009), western Australia (Eisenhauer et al. 1996), Aldabara Atoll (Braithwaite et al. 1973), and the Red Sea (Rohling et al. 2008), suggest that sea level was not constant *during* the LIG but instead underwent one or more falls and advances. The K09 GSL reconstruction showed some evidence of intra-LIG sea-level variations, but in that paper we did not investigate the detail of this variation or its robustness. Better understanding of these intra-interglacial sea level variations would be useful for testing hypotheses about, and models of, Greenland and Antarctic ice sheet variability in interglacial conditions, with potential application to future ice sheet changes.

In this paper, we extend the K09 methodology to investigate the robustness and magnitude of intra-LIG sea level variations and provide initial estimates of the associated rates of sea level change.

2 METHODOLOGY

The prior probability distribution for sea level adopted by K09 (Fig. 1) is a multivariate normal empirically derived from 250 alternative land-ice histories, each coupled with one of 72 alternative solid Earth models through a geophysical sea level model. The total land ice volume for each history was sampled from a probability distribution based upon the Lisiecki & Raymo (2005) oxygen isotope stack. The solid Earth models are distinguished on the basis of the adopted elastic lithospheric thickness and the viscosities of the upper and lower mantle regions. The geophysical modeling is based on a gravitationally self-consistent sea-level equation that takes into account viscoelastic deformation of the solid Earth and perturbations to the Earth’s gravitational field and rotational state. The sea-level theory takes accurate account of shoreline migration effects (Mitrovica & Milne 2003). To avoid predisposing the model to smooth sea level histories, the prior probability distribution allows relatively large swings in sea level, as can be seen by examining the peaks and lows in Fig. 1; we re-examine this assumption later.

Although the age model of our prior distribution for GSL is based upon the Lisiecki & Raymo (2005) timescale, the oxygen isotope curve does not unilaterally dictate the timescale of the posterior probability distribution. As one example of this limited influence, note that, while simple inference from Lisiecki & Raymo (2005) would place GSL at ~ -40 m at 115 ka, the K09 median posterior estimate is -0.5 m.

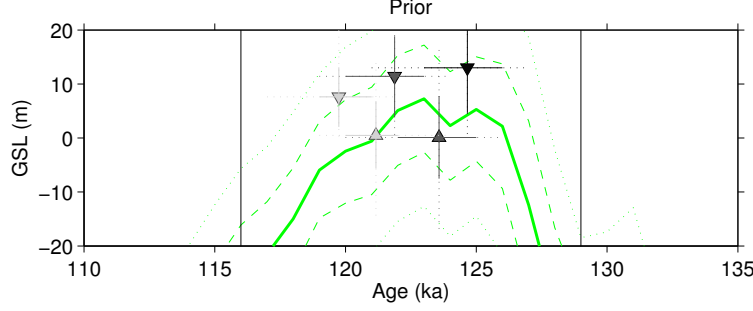


Figure 1. Prior probability distribution for mean global sea level (GSL). Resolved peaks (downward triangles) and troughs (upward triangles) are indicated. Grey tones indicate the probability of existence of peaks (black = 100%, white = 0%). Dashed and dotted error bars represent 67% and 95% confidence intervals, respectively. Because of the broad uncertainty in the prior, the prior expected ages of resolved peaks do not necessarily align with the peaks of the mean of the prior sea level distribution.

The K09 sea level database contains 108 distinct LIG sea level observations from 47 sites. Twenty-nine of these observations come from the Red Sea curve of Rohling et al. (2008), with a time scale adjusted to align (± 2.5 ky, 1σ) with that of Lisiecki & Raymo (2005). Although the uncertainties on these observations are relatively large ($\sim \pm 3$ m, 1σ), the Red Sea curve plays an important role in the analysis by anchoring the timescale. The other sites in the database are widely distributed geographically (see Fig. 1 of K09).

Let $f(g)$ represent global sea level over time g , \hat{s} the observed sea levels in the database, \hat{t} the measured ages corresponding to these observations, and t the corresponding true ages. After burn-in and thinning (Gilks et al. 1995), K09 generated 2,500 Markov Chain Monte Carlo (MCMC) samples from $P(t|\hat{s}, \hat{t})$, the posterior probability distribution of observation ages, conditioned upon the sea level and age observations. Each sample t_i of t defines a multivariate normal probability distribution for GSL conditioned upon sea level observations and the sampled ages, with mean $\hat{f}_i(g)$ and covariance Σ_i , such that we can write $P(f(g)|\hat{s}, t_i) \sim \mathcal{N}(\hat{f}_i(g), \Sigma_i)$. Our notation distinguishes between (1) the measured sea levels \hat{s} and ages \hat{t} , as recorded in the database; (2) a particular set of MCMC samples of true observation ages t_i ; and (3) the GSL curve over time, conditional upon a particular MCMC sample of observation ages, $P(f(g)|\hat{s}, t_i)$.

For a particular sample, we consider GSL at a given time point g to be “well resolved” if two criteria are satisfied: (1) $P(f(g)|\hat{s}, t_i)$ has a posterior standard deviation $< 30\%$ of the standard deviation of its prior $P(f(g))$ and (2) in the analysis employing the full database, the standard deviation of all $\hat{f}_i(g)$ is less than 10 m. The second criterion limits our focus to the time interval 129–116 ka. This definition of “well resolved” is slightly different from that of K09, which employed only the first criterion (see Fig. 4 of K09). Moreover, the definition is more

conservative, as it excludes an ambiguous pre-129 ka highstand that is highly contingent on the particular sampled values of t_i and separated from the body of the highstand by a well-resolved interval with $GSL < -15$ m.

For each sample t_i , we take 100 values from $P(f(g)|\hat{s}, t_i)$, considering only those time points g that are well resolved. For a particular value from $P(f(g)|\hat{s}, t_i)$, we identify the broad LIG highstand as the interval between 140 and 105 ka bounded by intervals during which GSL is greater than or equal to its present level. We identify the peaks and troughs of GSL that are well-resolved within this interval. Fig. 2 shows one example, in which the highstand extends from 126 to 113 ka, and two peaks and one trough are well-resolved.

To test our methodology, we evaluated it using twenty pseudoproxy data sets, described in the Supporting Information accompanying K09. To generate each data set, a known (randomly-generated) sea level history was sampled with pseudoproxy observations at the same locations and with the same characteristic sea level and age uncertainties as the actual observations in the database. The resulting analysis (Fig. S-1) suggests that the methodology presented here performs reasonably well: 57% of the data sets have true maximum rates of intra-LIG sea level change in excess of the projected 50% probability exceedance values; 52% of the data sets have true sea level maxima in excess of the projected 50% probability exceedance values; and 75% of the data sets have true sea level low-to-high swings in excess of the projected 50% probability exceedance values. The analysis does appear to overestimate the uncertainty in its projection of the sea level maxima for the pseudoproxy data; in all twenty of the data sets, the true sea level maximum falls between the 54% probability and 32% probability exceedance values.

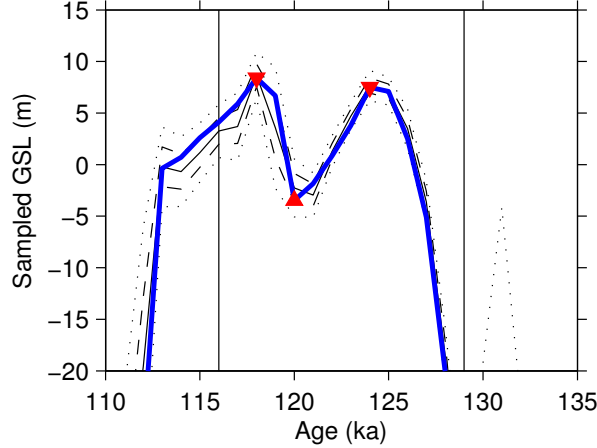


Figure 2. Peak identification example. The black curves show a distribution for GSL conditional upon a particular sample from the probability distribution for observation ages (solid: mean; dashed: 67% confidence interval; dotted: 95% confidence interval). The blue curve shows a single subsample from this distribution. The triangles indicate the identified peaks and lows of this subsample.

3 RESULTS

3.1 Main analysis

Figs. 3a and 4 (red line) and Tables 1–3 summarize some of the main results of our probabilistic assessment. Within the LIG window shown in Fig. 3, two peaks are identified with 98% confidence, a third with 63% confidence, and a fourth with 6% confidence (Table 1). In the age model constructed by our analysis, the best estimate of the age of the primary and (if they exist) secondary and tertiary peaks are 123–125 ka (quoted at the approximate 95% range), 116–122 ka and 116–118 ka.

We begin by considering the upper bound on GSL and the rate of GSL rise anywhere in the LIG time window. We find that, within the LIG period, it is extremely likely (95% probability)/likely (67%)/unlikely (33%)/extremely unlikely (5%) that the highest peak GSL well resolved by observations exceeded 6.4/7.7/8.8/10.9 m (Table 2). Moreover, we find that the fastest

Table 1. Probability of peak identification

<i>Number of peaks</i>	1	2	3	4	5
Full MCMC analysis	100%	98%	63%	6%	0%
≤ 2 Peaks	100%	95%	0%	0%	0%
No Red Sea (MCMC)	100%	100%	97%	70%	19%
No Red Sea	100%	100%	85%	40%	7%
Only Red Sea	100%	51%	3%	0%	0%
Only Best+RS	100%	98%	56%	5%	0%
Only Best–RS	100%	100%	79%	29%	3%
Prior	97%	66%	17%	1%	0%

Table 2. Maximum peak height (m)

<i>Exceedance probability</i>	95th	67th	50th	33rd	5th
Full MCMC analysis	6.4	7.7	8.2	8.8	10.9
≤ 2 Peaks	6.3	7.6	8.1	8.7	10.8
No Red Sea (MCMC)	6.8	8.5	9.3	10.2	14.0
No Red Sea	6.4	7.8	8.4	9.1	11.9
Only Red Sea	3.5	5.2	5.9	6.6	8.5
Only Best+RS	5.9	7.3	7.9	8.6	11.2
Only Best–RS	6.0	7.6	8.3	9.1	11.9
Prior	2.0	11.1	14.6	18.3	29.0

ky-average rate of GSL rise into and during the highstand exceeded 5.1/6.9/8.6/11.6 m/ky. These inferences differ slightly from our previous analysis (Kopp et al. 2009), which found extremely likely/likely/unlikely exceedance values of 6.6/8.0/9.4 m and 5.6/7.4/9.2 m/ky, because we limit our focus to the post-129 ka highstand clearly resolved by the data. That is to say, the current analysis excludes a possible ~ 132 ka peak whose resolution depends upon the interpretation of geochronological uncertainties and is separated from the main body of the LIG by a well-resolved interval of $\text{GSL} < -15$ m; see Fig. 3.

Considering only changes following the initial sea level peak, we find that the sea level low-to-high swing exceeded 1.1/7.8/11.2/15.1 m (Table 3), and that the maximum ky-average rate of GSL rise within the LIG exceeded 1.0/4.9/7.2/10.6 m/ky (Table 4).

3.2 Truncated analysis

The K09 prior probability distribution did not explicitly constrain the number of sea level peaks during the Last Interglacial, as we did not wish to be prescriptive in this regard. As a consequence, mismatched age models between different observations could lead to an overestimate of the number of peaks. One might therefore reasonably hold an implicit prior that judges fewer peaks to be more likely than more peaks. The absence of any known site

Table 3. Maximum intra-LIG low-to-high swing (m)

<i>Exceedance probability</i>	95th	67th	50th	33rd	5th
Full MCMC analysis	1.1	7.8	9.6	11.2	15.1
≤ 2 Peaks	0.0	4.4	8.2	10.2	14.5
No Red Sea (MCMC)	3.8	6.1	7.1	8.2	12.0
No Red Sea	3.0	7.0	8.5	10.1	15.5
Only Red Sea	0.0	0.0	0.1	2.7	8.5
Only Best+RS	0.8	8.4	10.3	11.8	15.6
Only Best–RS	2.0	5.9	7.3	9.0	14.1
Prior	0.0	0.0	6.1	10.9	23.9

Table 4. Maximum intra-LIG sea level rise rate (m/ky)

<i>Exceedance probability</i>	95th	67th	50th	33rd	5th
Full MCMC analysis	1.0	4.9	6.1	7.2	10.6
≤ 2 Peaks	0.0	3.3	5.0	6.4	9.9
No Red Sea (MCMC)	2.6	4.4	5.2	6.1	9.5
No Red Sea	2.1	4.8	5.8	6.9	10.9
Only Red Sea	0.0	0.0	0.1	2.3	7.2
Only Best+RS	0.8	5.2	6.5	7.6	10.8
Only Best−RS	1.3	3.8	5.0	6.2	10.2
Prior	0.0	0.0	5.0	8.5	17.6

with geomorphological indicators recording more than two sea level peaks supports this implicit prior. In the absence of a particular form for this prior, we conduct a sensitivity analysis employing a truncated uniform distribution for the number of peaks; i.e., we consider only the 37% of cases in which the models find ≤ 2 LIG sea level peaks (Fig. 3b and Fig. 4, blue line.)

The truncation has almost no effect on our estimate of peak sea level, which under the truncated prior exceeded 6.3/7.6/8.7/10.8 m (~ 10 cm less than in the untruncated analysis) (Table 2). It does somewhat reduce the maximum rate of rise into and during the LIG, which in this analysis exceeded 4.9/6.6/8.2/11.2 m/ky (0.3–0.4 m/ky slower). A second sea level peak during the LIG is resolved with 95% confidence (Table 1). Considering only changes following the initial sea level peak, the sea level low-to-high swing exceeded 0.0/4.4/10.2/14.5 m (Table 3); the maximum ky-average rate of GSL rise within the LIG exceeded 0.0/3.3/6.4/9.9 m/ky (Table 4).

3.3 Subset analyses

To assess the contribution of different data to our results, we conduct a number of analyses employing subsets of the full database. K09 conducted comprehensive subset analyses, in which the entire MCMC analysis, including consideration of geochronological uncertainties, was run upon limited data sets (see the Supplementary Information and Fig. S8 of K09). We consider one such subset, the K09 “no isotopes” subset, which excludes the Red Sea curve from the analysis. Here, we refer to this subset as the “No Red Sea (MCMC)” subset. We also consider a number of additional subsets, for which (for reasons of computational economy) we have not re-run the entire MCMC analysis but have instead retained the probability distributions for \mathbf{t}_i from the main analysis while using only the subset for the Gaussian process estimation of $P(f(g)|\hat{\mathbf{s}}, \mathbf{t})$. These subsets are:

- No Red Sea: all data except the Rohling et al. (2008) Red Sea curve,
- Only Red Sea: only the Red Sea curve,

- Only Best+RS: only Bahamas (Chen et al. 1991; Hearty et al. 2007), Bermuda (Muhs et al. 2002; Hearty et al. 2007), Western Australia (Murray-Wallace & Belperio 1991; Zhu et al. 1993; Stirling et al. 1995; Eisenhauer et al. 1996; Stirling et al. 1998; Hearty et al. 2007), Seychelles (Israelson & Wohlfarth 1999), Barbados (Schellmann & Radtke 2004), Oahu (Muhs et al. 2002; Hearty et al. 2007) and the Red Sea curve, and

- Only Best−RS: as above, but excluding the Red Sea curve.

The sites in the “Only Best” subsets are selected from the database to maximize overlap with the sites considered by Dutton & Lambeck (2012).

Results of the subset analyses are shown in Tables 1–4 and Fig. S-2. The Only Red Sea subset less clearly resolves multiple peaks (51% probability of a second peak) (Table 1), has a lower overall maximum height (exceeding 3.5/5.2/6.6/8.5 m; Table 2) and has a lower maximum rate of intra-LIG sea level variations (exceeding 0/0/2.3/7.2 m/ky; Table 4). Variations among the other subsets are relatively modest, with the notable exception that all the subsets excluding the Red Sea data have longer high stands and a greater likely number of peaks. With the exceptions of the Only Red Sea and No Red Sea (MCMC) subsets, all subsets yield maximum LIG GSL heights exceeding 5.9–6.4/7.3–7.8/8.6–9.1/10.8–11.9 m (Table 2). The No Red Sea (MCMC) subset yields higher exceedance values, and the Only Red Sea subset lower values. With the exception of the Only Red Sea subset, all yield a $\geq 95\%$ probability of at least two peaks (Table 1), and a maximum intra-LIG rate of sea level rise likely exceeding 3.8–5.2 m/ky, unlikely exceeding 6.1–7.6 m/ky, and extremely unlikely exceeding 9.5–10.9 m/ky (Table 4).

4 DISCUSSION AND CONCLUSIONS

K09 estimated with 95% confidence that the peak ky-averaged rate of GSL rise when GSL exceeded -10 m was greater than 5.6 m/ky, but that this rate was unlikely (33% probability) to have exceeded 9.2 m/ky. They cautioned that ky-averaged rates could not be used to place an upper bound on the fastest rate of sea level rise over shorter timescales. Moreover, as a few m equivalent eustatic sea level of ice in the Laurentide and/or Eurasian ice sheets likely remained on the planet when $\text{GSL} > -10$ m, these rates may have been dominated by ice loss from one of these ice sheets rather than from a currently extant ice sheet.

Focusing more specifically on intra-LIG sea level observations, if they can be resolved, provides more direct information about the behavior of the Greenland and Antarctic ice sheets during this period. Since the exceedance probabilities from the ≤ 2

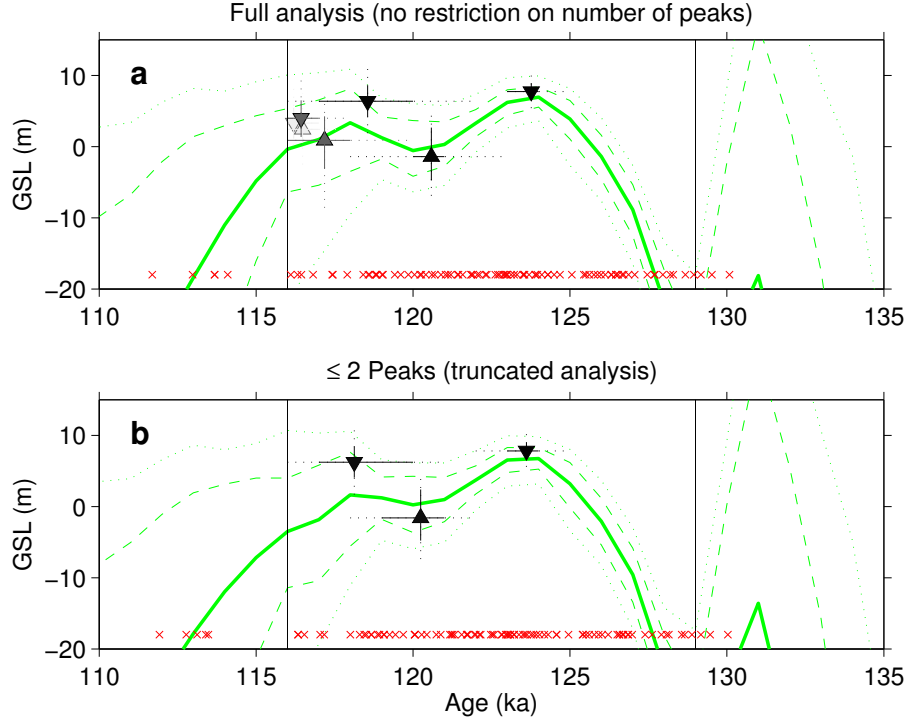


Figure 3. Resolved peaks (downward triangles) and troughs (upward triangles) of the LIG sea level curve. (a) Results of the full analysis. (b) Results with a truncated uniform prior limiting the number of peaks to ≤ 2 . Grey tones indicate the probability of peak existence (black = 100%, white = 0%). Solid, dotted, and dashed green lines indicate the mean GSL estimate and its 67% and 95% confidence intervals, respectively. Red crosses show the mean estimates of the ages of sea level observations.

peaks analysis are always less than or equal to those from the untruncated “full” analysis, we conservatively employ lower bounds from the former and upper bounds from the latter. We therefore conclude that it is extremely likely that our analysis resolves the existence of at least one sizable intra-LIG sea level fall and rise, likely one in excess of 4 m. Moreover, the sea-level rise following the lowstand occurred at a maximum ky-averaged rate that likely exceeded 3 m/ky, but was unlikely to have exceeded 7 m/ky and extremely unlikely (5% probability) to have exceeded 11 m/ky.

Both the rate and magnitude of the low-to-high GSL swing projected from this analysis are similar to those estimated for local changes in the Bahamas by Thompson et al. (2011), whose observations post-dated the compilation of the K09 database and were therefore not included in our analysis. Thompson et al. (2011) estimated that an initial peak of 4 m was followed by a low of ≤ 0 m and a high of 6 m, and that the minimum rate of change during this interval was 2.6 m/ky. The rates of rise estimated from our analysis are lower than the maximum century-average rates of sea level change at the Red Sea estimated by Rohling et al. (2008) (1.6 ± 0.8 m/century), but given both the difference in timescale (century- vs. millennial-average) and geographic scope (global

vs. Red Sea), the results are not necessarily inconsistent.

While ky-averaged rates cannot provide an upper bound on shorter-term rates, they can provide a lower bound. Satellite altimetry data indicate that, over the last twenty years, global mean sea surface height has risen by 3.1 ± 0.4 mm/y (Nerem et al. 2010); it is therefore likely that sub-millennial intervals of faster GSL rise occurred during the LIG.

Our analysis is limited by geochronological ambiguity among the timescales employed by Last Interglacial sea level researchers, which amounts to a ~ 2 ky disagreement on the timing of the LIG highstand between age models based upon open-system U/Th dates and those based upon closed-system U/Th dates (e.g., Thompson et al. 2011; Dutton & Lambeck 2012). The K09 analysis, extended here, applied a prior probability distribution based upon the Lisiecki & Raymo (2005) age model. Ongoing work is investigating the consequences of different prior age models, which could alter some of the rates presented here. The truncated “ ≤ 2 peaks” case allows some examination of the effects of geochronological ambiguity on rate estimates, since this truncation selects for samples from the probability distribution with observation ages that maximize coherence rather than increase the number of sea level peaks. This truncation has

a modest effect on estimates of rates of change, but does reduce estimates of the magnitude of intra-LIG sea level swings.

The Last Interglacial is an imperfect analogue for the twenty-first century. Under most scenarios, LIG-like polar temperatures will likely be achieved by the middle of the century and exceeded by the end of it. On the other hand, Earth's greater eccentricity during the Last Interglacial led to more intense summer insolation in the Northern Hemisphere and more protracted summer melt periods in the Southern Hemisphere (Huybers & Denton 2008). Van de Berg et al. (2011) suggest that insolation changes were responsible for ~45% of LIG Greenland melting. Thus it cannot be concluded that LIG-like polar temperatures alone would be sufficient to cause LIG-like ice sheet melt.

The cryosphere is a complex system with inherent stochasticity, and it is unclear to what extent identical climatic forcings would generate identical ice sheet responses. While the ~130 m GSL change between glacial low stands and interglacial high stands is deterministically related to climate, the few meters of difference between interglacials may or may not be. Reconstruction of globally integrated records akin to those of the LIG for earlier interglacials can help resolve this question. Leveraging the distinct spatio-temporal presentation of sea level patterns associated with different meltwater sources to reconstruct not just GSL but also changes in individual ice sheets should yield further insight. Despite these caveats, the record of LIG sea level variations suggests that the ice sheets currently extant are likely capable of sustaining rates of melting faster than those observed today for at least a millennium.

ACKNOWLEDGEMENTS

We thank the members of the PALSEA (Paleo-Constraints on Sea Level Rise) working group funded by Past Global Changes/IMAGES (International Marine Past Global Change Study) for helpful discussion. This research was supported by NSF grant ARC-1203415 to REK. FJS was supported by NSF EAR-1150145.

REFERENCES

- Andersen, K. K., Azuma, N., Barnola, J.-M., et al., 2004. High-resolution record of Northern Hemisphere climate extending into the last interglacial period, *Nature*, **431**, 147–151.
- Blanchon, P., Eisenhauer, A., Fietzke, J., & Liebetrau, V., 2009. Rapid sea-level rise and reef back-stepping at the close of the last interglacial highstand, *Nature*, **458**, 881–884.
- Braithwaite, C. J. R., Taylor, J. D., & Kennedy, W. J., 1973. The evolution of an atoll: the depositional and erosional

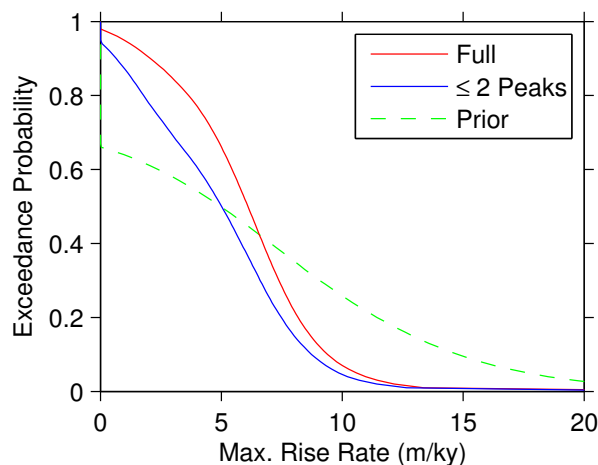


Figure 4. Exceedance probabilities (i.e., the probability the value exceeds a given level) for the maximum rate of sea level rise following the initial GSL peak. The red curve shows the results of the main analysis, while the blue curve shows the results with a truncated uniform prior limiting the number of peaks to ≤ 2 . The dashed green line indicates the prior.

- history of Aldabra, *Phil. Trans. Roy. Soc. B*, **266**, 307–340.
- CAPE-Last Interglacial Project Members, 2006. Last Interglacial Arctic warmth confirms polar amplification of climate change, *Quat. Sci. Rev.*, **25**, 1383–1400.
- Chen, J. H., Curran, H. A., White, B., & Wasserburg, G. J., 1991. Precise chronology of the last interglacial period: ^{234}U - ^{230}Th data from fossil coral reefs in the Bahamas, *Geol. Soc. Am. Bull.*, **103**, 82–97.
- Dutton, A. & Lambeck, K., 2012. Ice volume and sea level during the last interglacial, *Science*, **337**, 216–219.
- Eisenhauer, A., Zhu, Z. R., Collins, L. B., Wyrwoll, K. H., & Eichsttter, R., 1996. The Last Interglacial sea level change: new evidence from the Abrolhos islands, West Australia, *Geol. Rund.*, **85**, 606–614.
- Gilks, W. R., Richardson, S., & Spiegelhalter, D., 1995. *Markov Chain Monte Carlo in Practice: Interdisciplinary Statistics*, CRC Press.
- Hearty, P. J., Hollin, J. T., Neumann, A. C., O’Leary, M. J., & McCulloch, M., 2007. Global sea-level fluctuations during the Last Interglaciation (MIS 5e), *Quat. Sci. Rev.*, **26**, 2090–2112.
- Huybers, P. & Denton, G., 2008. Antarctic temperature at orbital timescales controlled by local summer duration, *Nat. Geosci.*, **1**, 787–792.
- Israelson, C. & Wohlfarth, B., 1999. Timing of the Last-Interglacial high sea level on the Seychelles Islands, Indian Ocean, *Quat. Res.*, **51**, 306–316.
- Kopp, R. E., Simons, F. J., Mitrovica, J. X., Maloof, A. C., & Oppenheimer, M., 2009. Probabilistic assessment of sea level during the last interglacial stage, *Nature*, **462**, 863–867.
- Kopp, R. E., Mitrovica, J. X., Griffies, S. M., Yin, J., Hay, C. C., & Stouffer, R. J., 2010. The impact of Greenland melt on local sea levels: a partially coupled analysis of dynamic and static equilibrium effects in idealized water-hosing experiments, *Clim. Change*, **103**, 619–625.
- Lisiecki, L. E. & Raymo, M. E., 2005. A Pliocene-

- Pleistocene stack of 57 globally distributed benthic $\delta^{18}\text{O}$ records, *Paleocean.*, **20**, PA1003.
- McKay, N. P., Overpeck, J. T., & Otto-Bliesner, B. L., 2011. The role of ocean thermal expansion in Last Interglacial sea level rise, *Geophys. Rev. Lett.*, **38**, L14605.
- Mitrovica, J. X. & Milne, G. A., 2003. On post-glacial sea level: I. General theory, *Geophys. J. Int.*, **154**, 253–267.
- Mitrovica, J. X., Gomez, N., Morrow, E., Hay, C., Latychev, K., & Tamisiea, M. E., 2011. On the robustness of predictions of sea level fingerprints, *Geophys. J. Int.*, **187**, 729–742.
- Muhs, D. R., Simmons, K. R., & Steinke, B., 2002. Timing and warmth of the Last Interglacial period: new U-series evidence from Hawaii and Bermuda and a new fossil compilation for North America, *Quat. Sci. Rev.*, **21**, 1355–1383.
- Murray-Wallace, C. & Belperio, A. P., 1991. The Last Interglacial shoreline in Australia – a review, *Quat. Sci. Rev.*, **10**, 441–461.
- Nerem, R. S., Chambers, D. P., Choe, C., & Mitchum, G. T., 2010. Estimating mean sea level change from the TOPEX and Jason altimeter missions, *Marine Geodesy*, **33**, 435–446.
- NOAA National Climatic Data Center, 2011. State of the climate: Global analysis for annual 2011, published online Dec. 2011, <http://www.ncdc.noaa.gov/sotc/global/2011/13>.
- Otto-Bliesner, B. L., Marshall, S. J., Overpeck, J. T., Miller, G. H., & Hu, A., 2006. Simulating Arctic climate warmth and icefield retreat in the Last Interglaciation, *Science*, **311**, 1751–1753.
- Overpeck, J. T., Otto-Bliesner, B. L., Miller, G. H., Muhs, D. R., Alley, R. B., & Kiehl, J. T., 2006. Paleoclimatic evidence for future ice-sheet instability and rapid sea-level rise, *Science*, **311**, 1747–1750.
- Rohling, E. J., Grant, K., Hemleben, C. H., Siddall, M., Hoogakker, B. A. A., Bolshaw, M., & Kucera, M., 2008. High rates of sea-level rise during the last interglacial period, *Nat. Geosci.*, **1**, 38–42.
- Schellmann, G. & Radtke, U., 2004. A revised morpho- and chronostratigraphy of the Late and Middle Pleistocene coral reef terraces on Southern Barbados (West Indies), *Earth-Sci. Rev.*, **64**, 157–187.
- Stirling, C. H., Esat, T. M., McCulloch, M. T., & Lambeck, K., 1995. High-precision U-series dating of corals from Western Australia and implications for the timing and duration of the Last Interglacial, *Earth Planet. Sci. Lett.*, **135**, 115–130.
- Stirling, C. H., Esat, T. M., Lambeck, K., & McCulloch, M. T., 1998. Timing and duration of the Last Interglacial: evidence for a restricted interval of widespread coral reef growth, *Earth Planet. Sci. Lett.*, **160**, 745–762.
- Thompson, W. G., Curran, H. A., Wilson, M. A., & White, B., 2011. Sea-level oscillations during the last interglacial highstand recorded by Bahamas corals, *Nat. Geosci.*, **4**, 684–687.
- Turney, C. S. M. & Jones, R. T., 2010. Does the Agulhas Current amplify global temperatures during super-interglacials?, *J. Quat. Sci.*, **25**, 839–843.
- van de Berg, W. J., van den Broeke, M., Ettema, J., van Meijgaard, E., & Kaspar, F., 2011. Significant contribution of insolation to Eemian melting of the Greenland ice sheet, *Nat. Geosci.*, **4**, 679–683.
- Zhu, Z. R., Wyrwoll, K. H., Collins, L. B., Chen, J. H., Wasserburg, G. J., & Eisenhauer, A., 1993. High-precision U-series dating of Last Interglacial events by mass spectrometry: Houtman Abrolhos Islands, western Australia, *Earth Planet. Sci. Lett.*, **118**, 281–293.

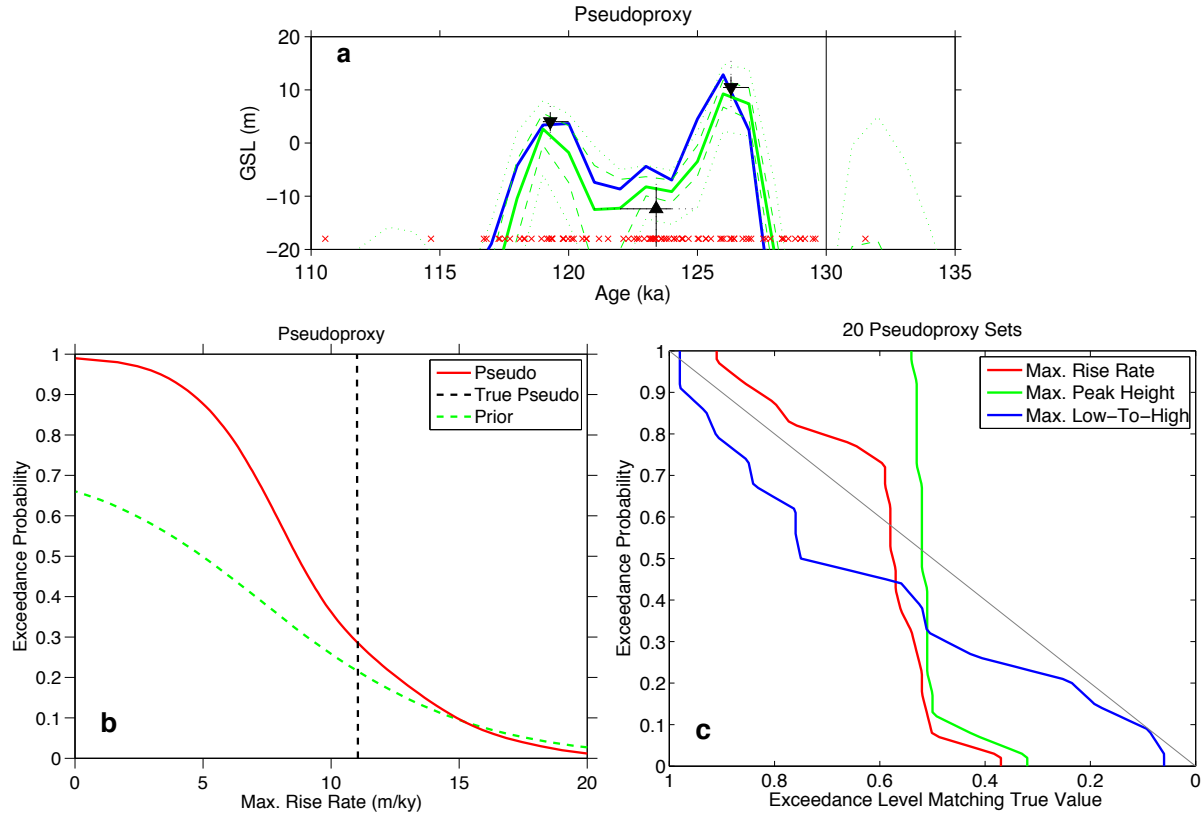


Figure S-1. Pseudoproxy analyses. (a,b) Analyses for one particular proxy data set. (a) Projected GSL distribution (green curve) and its 67% (dashed) and 95% (dotted) confidence intervals, true GSL (blue curve), identified peaks and troughs (triangles), and mean projection of observation ages (red crosses). (b) Exceedance probability for different rates of intra-LIG sea level rise (red), the prior (dashed green curve), and the known true value (dotted vertical line). (c) Probability, for 20 different pseudoproxy data sets, that the true value of a given statistic exceeded a given exceedance level. The statistics shown are maximum rate of intra-LIG sea level rise (red), maximum peak height (green), and maximum intra-LIG low-to-high sea level swing (blue). The grey curves shows a 1:1 line for comparison; values above this line reflect a projection underestimate, and values below this line an overestimate. For example, the green curve indicates that in all the pseudoproxy data sets, the true peak height fell between the 54% and 32% probability exceedance levels.

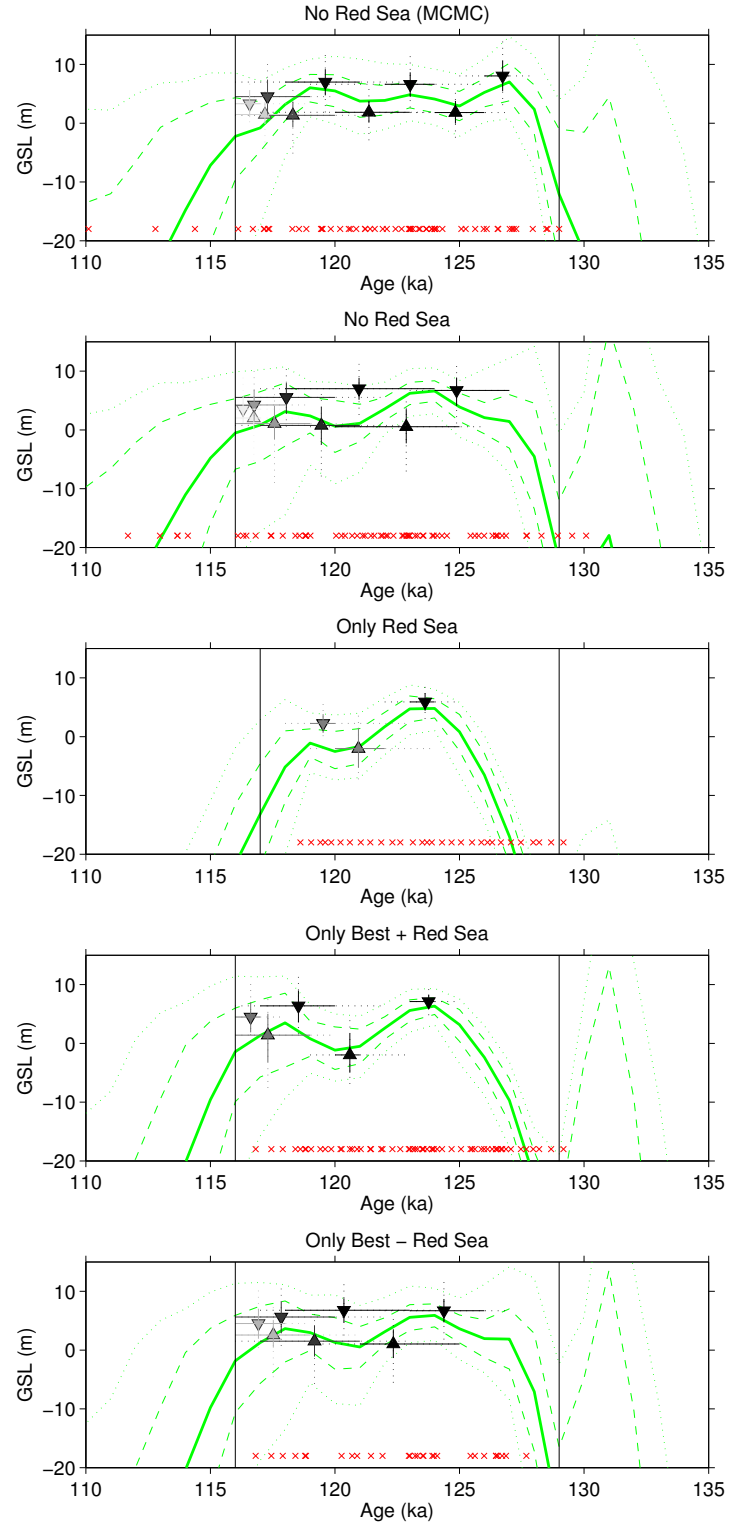


Figure S-2. Resolved peaks (downward triangles) and troughs (upward triangles) of the LIG sea level curve for subset analyses. Presentation as in Fig. 3.